

# A Hybrid Active/Passive Wrist Approach for Increasing Virtual Fixture Stiffness in Comanipulated Robotic Minimally Invasive Surgery

Caspar Gruijthuijsen<sup>1,2</sup>, Gianni Borghesan<sup>1,2</sup>, Dominiek Reynaerts<sup>1,2</sup>, and Emmanuel Vander Poorten<sup>1</sup>

**Abstract**—In Minimally Invasive Surgery (MIS), the incision point acts as a fulcrum about which the surgical instrument pivots. Most robotic MIS systems foresee procedures to carefully align the robot with the incision in the patient. Such procedures disrupt the normal workflow. This hampers the clinical translation of such assistive technology. In contrast, Backdrivable, Wristed (BW) robots, especially when operated as comanipulation devices, have a minimal impact on the traditional surgical workflow in MIS, as they are readily equipped with algorithms that automate fulcrum point estimation.

To improve safety, accuracy and/or task completion time, virtual fixtures can be implemented at the distal instrument tip, using an assistive BW system. This letter formalizes the problems related to such distal virtual fixtures. It then develops a hybrid active/passive wrist control strategy to improve the performance of virtual fixtures with BW systems while minimizing stability issues. Aside from an analytical example, experimental validation is added to show that the new algorithm increases the achievable stiffness of distal virtual fixtures.

**Index Terms**—Medical robots and systems, surgical robotics: laparoscopy, haptics and haptic interfaces

## I. INTRODUCTION

**T**HANKS to its small keyhole incisions, Minimally Invasive Surgery (MIS) has a number of distinct advantages for the patient, such as smaller scars, less pain, reduced risk of infection and faster recovery. At the same time, these incisions alter the surgeon's experience substantially. Long and slender instruments are needed to reach the targeted anatomy through access ports that are introduced at the different incisions. Each keyhole acts as a fulcrum about which a surgical instrument describes a pivoting motion. As such, it impacts, amongst others, the surgeon's motion Degrees of Freedom (DoFs), ergonomics, haptic sensation and psychomotor skills. Robotic systems developed to assist the surgeon have to take into account the kinematic constraints arising from this fulcrum point. These systems can be classified according to the approach they adopt for dealing with the fulcrum.

Manuscript received: Februari 24, 2019; Revised May 13, 2019; Accepted June 11, 2019.

This paper was recommended for publication by Editor Pietro Valdastri upon evaluation of the Associate Editor and Reviewers' comments. This work was supported by an internally funded project at KU Leuven (PRESLICE-3E160397).

<sup>1</sup>C. Gruijthuijsen, G. Borghesan, D. Reynaerts and E. Vander Poorten are with the Department of Mechanical Engineering, KU Leuven, Leuven, Belgium. [firstname.lastname@kuleuven.be](mailto:firstname.lastname@kuleuven.be)

<sup>2</sup>C. Gruijthuijsen, G. Borghesan, D. Reynaerts are members of Flanders Make, Leuven, Belgium.

Digital Object Identifier (DOI): see top of this page.

The best known approach is the *Mechanical Remote Center of Motion* (MRCM), where a dedicated mechanical construction constrains the instrument to pass through the fulcrum. Such mechanisms require a calibration step to align the MRCM with the incision. Misalignment, due to improper calibration or patient motion, leads to excessive stresses on the body wall, potentially causing Trocar Site Herniation [1]. Many examples of MRCM systems exist, both for teleoperation, such as the da Vinci Surgical System (Intuitive Surgical, Sunnyvale, CA, USA) and the RAVEN-III (Applied Dexterity, Seattle, WA, USA), and for comanipulation, such as the Stryker Acrobot [2] or the Steady Hand and KU Leuven robots for retinal micro-surgery [3], [4].

To overcome misalignment problems arising from patient motion, mechanical systems featuring a *Local Center of Motion* (LCM) may be mounted on the body of the patient, directly at the incision site. Examples include the ViKY [5] and the MC<sup>2</sup>E [6] system. Although proper alignment is facilitated, the performance of these systems suffers from design constraints (in terms of size, weight, space occupancy) that follow from their body-mountable nature.

Another approach concerns *Virtual RCM* (VRCM) systems, which have excess DoFs that are employed to replace the mechanical constraint by a soft, programmed constraint. The position of the fulcrum point w.r.t. the robotic system has to be determined using an alignment procedure, such as in [7], after which the constraint is maintained through coordinated control of the joints. The most notable VRCM example is DLR's teleoperated MIRO robot [8].

*Passive RCM* (PRCM) systems, typically used for robotic endoscope holders, contain active DoFs that realize a pivoting motion about an MRCM, in such a way that the DoFs most naturally map to the endoscope's tilt, pan and zoom motions. This yields a very simple controller. A calibration phase is needed to align the RCM to the incision point. To ensure that no excessive stresses occur in case of misalignment, the instrument is connected to the system through two orthogonal passive revolute joints. Thus, the severity of misalignments is reduced to small disturbances in the instrument position control. The EVOLAP [9] and LapMan [10] are examples of such approach.

The last category consists of *Backdrivable, Wristed* (BW) systems. Here, the instrument is connected to a wrist at the end of a backdrivable multi-DoF robotic arm. The wrist is able to act as a passive, spherical joint, such that the fulcrum constraint cannot be violated. The arm may have a

SCARA topology, such as in the AESOP system [11], or an anthropomorphic topology, as for Apollo [12].

In a comanipulation context, where the instrument is synergistically manipulated by both the surgeon and robot, BW systems deal with the fulcrum constraint in a way that closely resembles surgical practice without robotic assistance. The surgeon stands next to the patient and relies on the same hand-eye coordination as in traditional MIS. He/she can freely manipulate the instrument (with some small added impedance), even in case of power breakdown. A time-consuming alignment procedure is avoided. Instead, the location of the incision point can be estimated by automated routines as soon as the instrument is inserted [13], [14]. These routines can run continuously to accommodate for patient motion and incision point compliance. Latter approach minimizes changes to the current surgical workflow, which is favourable for translation to the clinic. Yet, in literature, few works focus on comanipulated BW systems.

This work shows how to improve the quality of assistive techniques that can be offered with a BW robot, such as virtual fixtures. First, related work will be discussed in Sec. II. The adverse effects of the fulcrum point on distal virtual fixtures are analysed in Sec. III. Sec. IV then proposes a method to optimally compensate for these effects, followed by experimental results and a discussion in Sec. V. Sec. VI summarizes the conclusions.

## II. RELATED WORK

Virtual Fixtures (VFs), otherwise known as Active Constraints, were first defined by Rosenberg [15] as virtual sensory overlays upon a user's perception, typically haptic perception. Haptic VFs provide an interesting alternative to visual feedback when physical constraints are present, because they do not rely on unnatural sensory substitution [16]. As such, they can improve safety, accuracy and task completion time. An extensive classification and discussion on VFs can be found in [17], [18].

Although VFs are a well-documented topic, only few works investigated the application of VFs at the distal tip of a surgical instrument in a comanipulation scenario: distal stiffness VFs were studied in [19], [20] and distal damping VFs in [21]. The particularity here is that the fulcrum point introduces a variable transformation of the kinematics and dynamics of the distal VF towards the proximal side, where the instrument is controlled by a robot (and the surgeon).

Vitrani *et al.* pointed out that two different approaches can be adopted to realize a certain desired VF behaviour: an *Active Wrist* (AW) and a *Passive Wrist* (PW) approach [19]. With the AW approach, the proximally located robot exerts a wrench that is equivalent to the force generated by the VF at the distal end. Thanks to the backdrivability of the robot, the fulcrum constraint will be satisfied. This approach does not depend on knowledge of the fulcrum position, but requires an active arm to produce forces, as well as rotational actuators in the wrist to produce moments. Conversely, the PW approach does not need rotational actuators in the wrist. Instead, it treats the pivoting instrument as an idealized mechanical lever

and solves the force equilibrium over the fulcrum to find the proximal force that is equivalent to the targeted distal force. Note that the PW approach has the interesting property that it renders VFs without adding reaction forces to the fulcrum. This approach relies on knowledge of the fulcrum position. Despite the fundamental differences between AW and PW control strategies, no significant difference in user experience nor in user performance has been reported. This raises the question whether it can be advantageous to combine both strategies for robots with wrist actuators, in order to optimize performance in challenging control conditions. This will be addressed in Section IV.

Most research efforts on VFs focus on VF localization and VF stability. Localization boils down to a simple registration problem in static scenarios where preoperative data is available [2], [22]. If the environment is deformable or dynamic, more advanced VF localization methods are required, based on intraoperative sensing, such as [23], [24], [20].

Recent work by Colonnese *et al.* provides a rigorous discussion on stable haptic rendering [25]. VF stability is often guaranteed through the effective but conservative passivity criterion. It states that, at no point in time, the energy that is extracted from a system can be larger than the system's initial energy. The range of impedances that can be passively rendered is typically referred to as the Z-width. A number of approaches exist to extend the Z-width: control methods such as virtual couplings or passivity observers and passivity controllers (PO/PC), or hardware solutions such as controllable physical dampers. All strive to balance energy leaks up to a level that the leak is dissipated by physical damping elements [26]. Passivity can also be ensured by restricting the controller to dissipative elements [27].

This work proposes a hybrid AW/PW control approach that optimizes the use of actuator redundancy to increase the Z-width. The proposed method proceeds by ensuring that the physical damping of the individual actuators is optimally exploited and the passivity of all actuators is respected while doing so. Before describing the proposed control approach in Section IV, the next section will first analyse the implications and specific challenges of the presence of a fulcrum point on rendering distal VFs. It also describes the opportunities that reside in the presence of actuator redundancy.

## III. FULCRUM EFFECT ON STIFFNESS RENDERING

The incision point, acting as a fulcrum, causes a configuration-dependent transformation of forces and motions from proximal to distal instrument end. Gallagher *et al.* described the cognitive and perceptual difficulties the surgeon experiences because of this *fulcrum effect* [28]. Later work by Sülzenbrück *et al.* studied the kinematic and dynamic transformations more formally, investigating the underlying motor and cognitive processes and how they dominate errors in goal-directed movements [29]. Nisky *et al.* show that the fulcrum effect biases the perception of haptic information, such as the stiffness of a VF [30]. Robotic systems are also affected by the fulcrum effect when, for example, a VF is to be rendered distally. The following provides a mathematical analysis of this phenomenon.

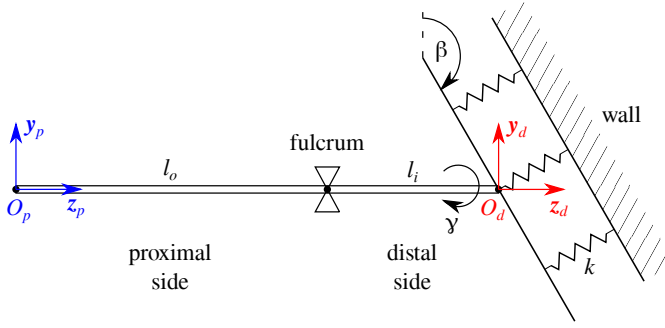


Figure 1: Definition of the distal and proximal instrument frames and parameters. The distal instrument tip at  $O_d$  is in contact with a virtual wall of stiffness  $k$ , which is rotated with respect to the distal frame by angles  $\beta$  and  $\gamma$ . A robotic manipulator is expected to hold the instrument at the proximal end  $O_p$ .

### A. Fulcrum Model

The fulcrum, visualized in Fig. 1, can be modelled as:

$$\frac{\delta p_{p,x}}{l_o} = -\frac{\delta p_{d,x}}{l_i} = -\delta \theta_{p,y} = -\delta \theta_{d,y}, \quad (1)$$

$$\frac{\delta p_{p,y}}{l_o} = -\frac{\delta p_{d,y}}{l_i} = \delta \theta_{p,x} = \delta \theta_{d,x}, \quad (2)$$

$$\delta p_{p,z} = \delta p_{d,z}, \quad (3)$$

$$\delta \theta_{p,z} = \delta \theta_{d,z}. \quad (4)$$

In these equations,  $l_o$  is the instrument length outside the patient and  $l_i$  the instrument length inside. The infinitesimal translation  $\delta \mathbf{p}$  and infinitesimal rotation  $\delta \boldsymbol{\theta}$  are expressed w.r.t. the respective proximal and distal instrument coordinate frames  $\{p\}$  and  $\{d\}$ . Equations (1) and (2) show how motion is scaled in  $x$ - and  $y$ -direction, whereas it remains unaltered in the  $z$ -direction, according to (3) and (4). The lever ratio  $a$  relates  $l_o$  to  $l_i$  as:

$$a = \frac{l_i}{l_o}. \quad (5)$$

From these relations, the fulcrum mapping between proximal and distal displacements (and reciprocally forces) can be summarized as:

$$\delta \mathbf{p}_d = \mathbf{J}_f \delta \mathbf{p}_p, \quad (6)$$

with

$$\mathbf{J}_f = \begin{bmatrix} -a & 0 & 0 \\ 0 & -a & 0 \\ 0 & 0 & 1 \end{bmatrix}. \quad (7)$$

### B. Actuator Redundancy

The fulcrum introduces a coupling between the linear and rotational DoFs in the plane perpendicular to the instrument, reducing the total number of instrument DoFs from six to four. Consequently, a BW device manipulating a surgical instrument with six active DoFs has two redundant actuators.

For simplicity, but without loss of generality, it is assumed that the wrist position is controlled by *linear* actuators, while in the wrist itself moments are generated by *rotational* actuators. These linear and rotational actuators act in parallel in the plane perpendicular to the instrument axis. Therefore, a proximal force  $\delta \mathbf{f}_p$  can be transformed into an equivalent proximal wrench  $\delta \mathbf{w}_p$ , using wrist weighting factors  $w_x, w_y$  to distribute the effort over the redundant actuators:

$$\delta \mathbf{w}_p = \mathbf{J}_p^T \delta \mathbf{f}_p, \quad (8)$$

with

$$\mathbf{J}_p = \begin{bmatrix} w_x & 0 & 0 & 0 & -l_o(1-w_x) & 0 \\ 0 & w_y & 0 & l_o(1-w_y) & 0 & 0 \\ 0 & 0 & 1 & 0 & 0 & 0 \end{bmatrix}. \quad (9)$$

### C. Stiffness Distortion

A VF, whether it is a forbidden region VF or a guidance VF [18], can be represented by a virtual wall with a normal that instantaneously coincides with the desired force direction. This wall of stiffness  $k$  can be expressed in the distal coordinate frame as:

$$\mathbf{K}_d = \mathbf{R}_d \text{diag}(0, 0, k) \mathbf{R}_d^T, \quad (10)$$

with the distal wall rotation  $\mathbf{R}_d = \mathbf{R}_z(\gamma) \mathbf{R}_x(\beta)$  defined by the wall inclination angle  $\beta$  and the axial rotation angle  $\gamma$ , as in Fig. 1.  $\mathbf{R}_i$  is a 3D rotation matrix about the axis  $i$ . Using the fulcrum mapping  $\mathbf{J}_f$ , this stiffness matrix can be mapped to the proximal side:

$$\mathbf{K}_p = \mathbf{J}_f^T \mathbf{K}_d \mathbf{J}_f. \quad (11)$$

The eigendecompositions of the symmetric, rank-1 stiffness matrices  $\mathbf{K}_d$  and  $\mathbf{K}_p$  reveal the effect of the fulcrum mapping on the stiffness:

$$\mathbf{K}_d = \mathbf{R}_d \text{diag}(0, 0, k_d) \mathbf{R}_d^T = \mathbf{R}_d \text{diag}(0, 0, k) \mathbf{R}_d^T, \quad (12)$$

$$\mathbf{K}_p = \mathbf{R}_p \text{diag}(0, 0, k_p) \mathbf{R}_p^T = s_f \mathbf{R}_p \text{diag}(0, 0, k) \mathbf{R}_p^T, \quad (13)$$

↓

$$\mathbf{K}_p = s_f \mathbf{R}_p \mathbf{R}_d^T \mathbf{K}_d \mathbf{R}_d \mathbf{R}_p^T = s_f \mathbf{R}_f \mathbf{K}_d \mathbf{R}_f^T, \quad (14)$$

where  $s_f$  represents the fulcrum scaling factor:

$$s_f = a^2 \sin^2 \beta + \cos^2 \beta \quad (15)$$

and  $\mathbf{R}_f$  the fulcrum rotation matrix:

$$\mathbf{R}_f = \mathbf{R}_p \mathbf{R}_d^T. \quad (16)$$

From (14), it can be seen that the fulcrum causes a distortion of the stiffness from distal to proximal side, in both magnitude ( $s_f$ ) and direction ( $\mathbf{R}_f$ ). This is illustrated in Fig. 2.

In scenarios where the instrument is deeply inserted ( $a \gg 1$ ) and approximately parallel to the virtual wall ( $\beta \rightarrow \frac{\pi}{2}$ ), it can be seen from (15) that the magnitude of the proximal stiffness  $k_p = s_f k$  is substantially larger than the distal stiffness  $k$ . Such

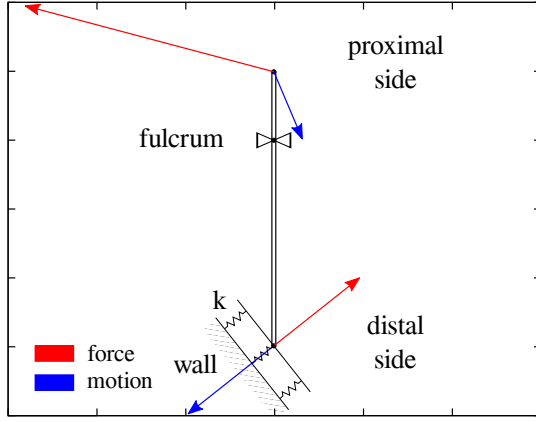


Figure 2: Magnitude and direction distortion of a distal stiffness  $k$  towards the proximal side of the instrument for  $a > 1$ .

scenario is common for real VF applications and challenging from a control perspective.

With the PW control approach, only pure forces are available at the proximal instrument end. In case this control strategy is used to render the distal stiffness  $k$ , stability issues could easily occur for large  $a$ , as the (linear) proximal stiffness is proportional to  $a^2$ , making it reach infinity upon full instrument insertion ( $l_o \rightarrow 0$ ). However, with the AW control approach, moments from rotational actuators are available at the proximal instrument end. This makes the impact of the insertion depth less pronounced: a distal stiffness  $k$  projected to the proximal rotational DoFs is proportional to  $a^2 l_o^2 = l_i^2$ . Thus, a full instrument insertion will yield a finite proximal stiffness with the AW approach.

In summary, the AW control strategy outperforms the PW strategy for  $a \gg 1$ . These observations, together with the fact that PW control is possible without hardware alterations whenever AW control is available, motivate the hybrid AW/PW control strategy.

#### IV. HYBRID AW/PW CONTROL

This section develops an algorithm to determine the optimal combination of the AW control strategy (which generates moments) and PW control strategy (where this is not the case). The resulting combination is governed by the choice of wrist weighting factors  $w_x$  and  $w_y$  from (9) and will depend on the pose of the haptic device, the individual actuator properties and the instrument insertion depth. In the following, it is shown how the optimal factors  $\hat{w}_x$  and  $\hat{w}_y$  can be selected such that the Z-width, or maximum passive stiffness, of the entire system is maximized.

##### A. Optimization of Wrist Weighting Factors

A number of preliminaries are necessary, before the optimization problem can be formulated. The passivity criterion from Colgate and Schenkel [31], states that, without virtual damping, the maximum passive stiffness for a virtual wall is limited by the physical damping  $b$  in the system and by the time step  $T$ :

$$\frac{2b}{T} \geq k. \quad (17)$$

Later work by Miller *et al.* shows how to adapt this expression in case the physical damping is present in joint space, instead of in task space [32]. Taking  $b_q$  as the joint space damping, (17) becomes:

$$\frac{2b_q}{T} \geq \mathbf{J}^T \frac{2b}{T} \mathbf{J} \geq \mathbf{J}^T k \mathbf{J}, \quad (18)$$

where  $\mathbf{J}$  is the differential mapping from task to joint space. This expression can be extended to the multi-DoF case:

$$\frac{2\mathbf{B}_q}{T} \geq \mathbf{J}^T \mathbf{K} \mathbf{J}, \quad (19)$$

with  $\mathbf{B}_q$  the joint space damping matrix and  $\mathbf{K}$  the task space stiffness matrix. This corresponds to the requirement that the matrix difference  $\frac{2\mathbf{B}_q}{T} - \mathbf{J}^T \mathbf{K} \mathbf{J}$  is positive semi-definite.

Intuitively,  $\frac{2\mathbf{B}_q}{T}$  can be interpreted as the available joint space stiffness, i.e., the upper limit on the stiffness that can be rendered without encountering stability issues. Thus, for ease of interpretation, the available stiffness  $\mathbf{K}_a$  is introduced:

$$\mathbf{K}_a = \frac{2\mathbf{B}_q}{T}. \quad (20)$$

The task space stiffness matrix for a virtual wall of stiffness  $k$  is defined as:

$$\mathbf{K} = \mathbf{K}_d \quad (21)$$

and the mapping  $\mathbf{J}$  from the distal joint space, via the fulcrum, to the robot joint space is:

$$\mathbf{J} = \mathbf{J}_f \mathbf{J}_p \mathbf{J}_r, \quad (22)$$

with  $\mathbf{J}_r$  the Jacobian of the BW haptic manipulator. Now, the joint space stiffness matrix for the virtual wall can be written as:

$$\mathbf{K}_w = \mathbf{J}_r^T \mathbf{J}_p^T \mathbf{J}_f^T \mathbf{K}_d \mathbf{J}_f \mathbf{J}_p \mathbf{J}_r. \quad (23)$$

The optimization problem to be solved becomes:

$$(\hat{w}_x, \hat{w}_y) = \arg \max_{(w_x, w_y)} k, \quad (24)$$

$$\text{s.t. } \mathbf{K}_a \succeq \mathbf{K}_w. \quad (25)$$

This problem can be simplified by resorting to a geometric interpretation. The symmetric, positive semi-definite matrices  $\mathbf{K}_a$  and  $\mathbf{K}_w$  can be associated with ellipsoids:

$$\varepsilon_{\mathbf{K}_a} = \{\mathbf{x} \mid \mathbf{x}^T \mathbf{K}_a^{-1} \mathbf{x} \leq 1\}, \quad (26)$$

$$\varepsilon_{\mathbf{K}_w} = \{\mathbf{x} \mid \mathbf{x}^T \mathbf{K}_w^{-1} \mathbf{x} \leq 1\}. \quad (27)$$

For these ellipsoids, the semi-axes and their lengths correspond, respectively, to the eigenvectors and square roots of the eigenvalues of the associated matrices. The following property holds [33]:

$$\mathbf{K}_a \succeq \mathbf{K}_w \Leftrightarrow \varepsilon_{\mathbf{K}_w} \subseteq \varepsilon_{\mathbf{K}_a}. \quad (28)$$

Since  $\mathbf{K}_a$  is generally diagonal, the semi-axes of  $\epsilon_{\mathbf{K}_a}$  are aligned with the axes  $\mathbf{e}_{qi}$  of the joint space reference frame.  $\mathbf{K}_w$  is a rank-1 matrix and thus has a single non-zero eigenvalue:

$$k_w = sk, \quad (29)$$

with  $s$  a positive scaling factor, corresponding to the eigenvector  $\mathbf{v}$ . Therefore,  $\epsilon_{\mathbf{K}_w}$  represents a line along  $\mathbf{v}$ , of which the length is proportional to  $\sqrt{k}$ . This is illustrated in Fig. 3.

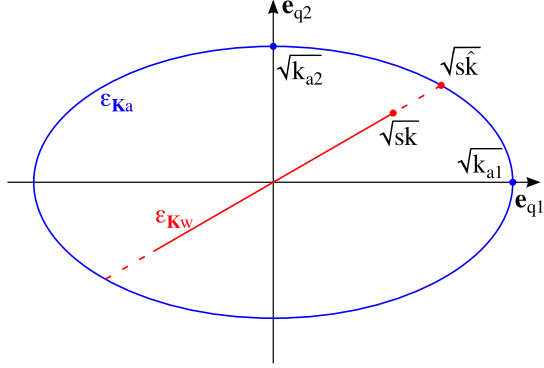


Figure 3: The ellipsoids  $\epsilon_{\mathbf{K}_a}$  and  $\epsilon_{\mathbf{K}_w}$ , respectively defined by the eigenvalues  $(k_{a1}, k_{a2})$  of  $\mathbf{K}_a$  and  $(sk, 0)$  of  $\mathbf{K}_w$ . The dashed red line shows the effect on  $\epsilon_{\mathbf{K}_w}$  if the maximum passive wall stiffness  $\hat{k}$  were used. This 2D representation can be readily extended to higher dimensions.

The Z-width, or maximum passive wall stiffness  $\hat{k}$ , can now be determined by plugging the position of the extremity of  $\epsilon_{\mathbf{K}_w}$  into the equation of  $\epsilon_{\mathbf{K}_a}$ :

$$\left( \sqrt{s\hat{k}} \frac{\mathbf{v}}{\|\mathbf{v}\|} \right)^T \mathbf{K}_a^{-1} \left( \sqrt{s\hat{k}} \frac{\mathbf{v}}{\|\mathbf{v}\|} \right) = 1. \quad (30)$$

An expression for  $\mathbf{v}$  can be found by re-evaluating (10) and (23):

$$\mathbf{K}_w = \mathbf{J}_r^T \mathbf{J}_p^T \mathbf{J}_f^T \mathbf{R}_d \text{diag}(0, 0, k) \mathbf{R}_d^T \mathbf{J}_f \mathbf{J}_p \mathbf{J}_r, \quad (31)$$

$$= k \mathbf{J}_r^T \mathbf{J}_p^T \mathbf{J}_f^T \mathbf{R}_d \mathbf{e}_z \mathbf{e}_z^T \mathbf{R}_d^T \mathbf{J}_f \mathbf{J}_p \mathbf{J}_r, \quad (32)$$

$$= k \mathbf{v} \mathbf{v}^T, \quad (33)$$

with

$$\mathbf{v} = \mathbf{J}_r^T \mathbf{J}_p^T \mathbf{J}_f^T \mathbf{R}_d \mathbf{e}_z. \quad (34)$$

It is straightforward to show that  $\mathbf{v}$  is the eigenvector of  $\mathbf{K}_w$ , corresponding to the eigenvalue

$$k_w = k(\mathbf{v} \cdot \mathbf{v}). \quad (35)$$

*Proof.*

$$\mathbf{K}_w \mathbf{v} = k \mathbf{v} \mathbf{v}^T \mathbf{v} = k \mathbf{v}(\mathbf{v} \cdot \mathbf{v}) = k(\mathbf{v} \cdot \mathbf{v}) \mathbf{v}. \quad (36)$$

□

Comparing (29) and (35) yields:

$$s = \mathbf{v} \cdot \mathbf{v}. \quad (37)$$

After substituting (37) in (30), an expression for  $\hat{k}$  can be obtained:

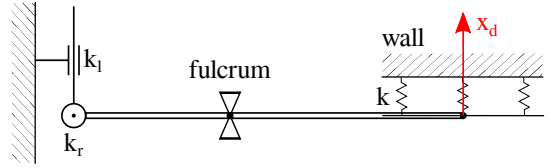


Figure 4: Simple 1D example with a virtual wall of stiffness  $k$  and two actuators that are able to render a linear stiffness  $k_l$  and a rotational stiffness  $k_r$ .

$$\hat{k} = (\mathbf{v}^T \mathbf{K}_a^{-1} \mathbf{v})^{-1}. \quad (38)$$

The optimization problem from (24)-(25) can now be formulated as:

$$(\hat{w}_x, \hat{w}_y) = \arg \max_{(w_x, w_y)} \hat{k} = \arg \min_{(w_x, w_y)} \mathbf{v}^T \mathbf{K}_a^{-1} \mathbf{v}. \quad (39)$$

In the appendix, an analytical solution to this problem is derived.

### B. Analytical Example

Consider a 1D task space, with a virtual wall of stiffness  $k$  perpendicular to the  $x_d$ -direction, as in Fig. 4. In joint space, this corresponds to one linear actuator with an available stiffness of  $k_l$  and one rotational actuator with an available stiffness of  $k_r$ . The involved Jacobians and stiffness matrices are:

$$\begin{aligned} \mathbf{J}_f &= [-a], & \mathbf{J}_p &= [w_x \quad l_o(w_x - 1)], & \mathbf{J}_r &= \mathbf{I}, \\ \mathbf{K}_d &= [k], & \mathbf{K}_a &= \text{diag}(k_l, k_r). \end{aligned} \quad (40)$$

Plugging (40) in (23) and solving the result for its eigenvalues and eigenvectors yields  $k_w$  and  $\mathbf{v}$ :

$$k_w = ka^2 w_x^2 + kl_i^2 (w_x - 1)^2, \quad (41)$$

$$\mathbf{v} = [aw_x \quad l_i(w_x - 1)]^T. \quad (42)$$

Using (40)-(42), the solution to the optimization problem from (39) can be found, yielding the maximum passive wall stiffness  $\hat{k}$  and the optimal wrist weighting factor  $\hat{w}_x$ :

$$\hat{k} = \frac{k_l}{a^2} + \frac{k_r}{l_i^2}, \quad (43)$$

$$\hat{w}_x = \left( 1 + \frac{k_r}{l_o^2 k_l} \right)^{-1}. \quad (44)$$

This result demonstrates that  $k_r$  and  $k_l$  can be interpreted as parallel springs, scaled by the configuration-dependent parameters  $a$  and  $l_i$ . Such springs reinforce each other, creating an opportunity to realize a higher passive wall stiffness  $\hat{k}$ . At the same time, (44) confirms the intuition that AW control ( $w_x \rightarrow 0$ ) takes the upper hand upon deep insertion ( $l_o \rightarrow 0$ ), and vice versa. Also, when  $k_r$  is large, owing to high physical damping in the rotational DoF,  $w_x \rightarrow 0$  and the AW approach is favoured. Conversely, PW control is advantageous when  $k_l$  is large.

## V. EXPERIMENTAL RESULTS & DISCUSSION

### A. Experimental Setup

The hybrid AW/PW method was implemented for the Virtuose6D (Haption SA, Laval, France), a 6-DoF haptic device. A dummy instrument was connected to the wrist of the device and inserted through a mechanical fulcrum, as can be seen in see Fig. 5. The system generated a horizontal virtual wall at the distal tip of the instrument.

### B. Optimization of Wrist Weighting Factor

Fig. 6 shows a typical graph for  $\hat{k}$  as a function of the insertion depth and the wrist weighting factor. To facilitate the visual interpretation of the results, the orientation of the reference frames with respect to the virtual wall was chosen such that  $\hat{k}$  is only dependent on a single wrist weighting factor  $w = w_x$ . This does not affect the generality of the results, as such reference frames can always be chosen.

The magenta line in Fig. 6 marks the optimal wrist weighting factor  $\hat{w}$  at each insertion depth. The green line shows the profile of  $\hat{k}$  as function of  $w$  for an insertion of 50%. It can be seen that around this insertion depth, there is a clear added value in combining AW and PW control. For this particular robot pose, the hybrid control raises the stiffness by 25% compared to PW and by 50% compared to AW. The figure shows how  $\hat{k}$  drops with deeper insertion, especially for PW control. AW is affected to a lesser extent by the insertion depth. At full insertion, AW can still deliver a non-zero  $\hat{k}$ , while for PW  $\hat{k}$  drops to zero. Consequently, the hybrid controller is pushed towards pure AW control at this insertion depth. At shallow depths, it becomes interesting to raise the share of PW control. The added value of the hybrid control as compared to either of the individual methods is here less pronounced though.

Similar graphs can be used to define a fixed  $w$  that is locally optimal in a predefined workspace, along with the maximum passive stiffness in that workspace. Such graphs can also be used as a design tool for studying the achievable stiffness of haptic devices. Alternatively, it is possible to optimize  $w$  in real-time, and concurrently  $\hat{k}$ , as function of the insertion depth and the comanipulator pose. This way, the virtual wall stiffness

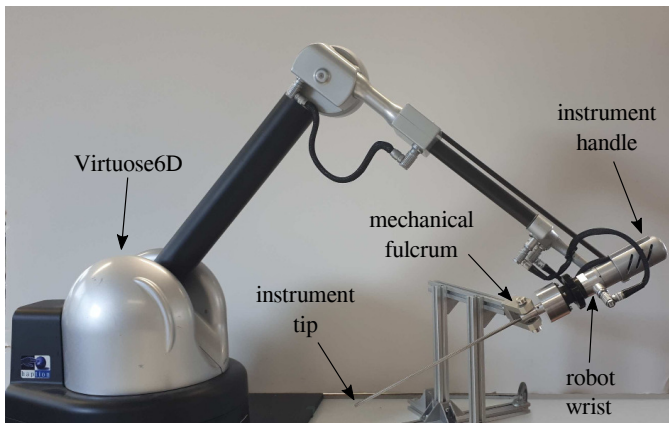


Figure 5: Virtuose6D configuration for virtual wall experiment.

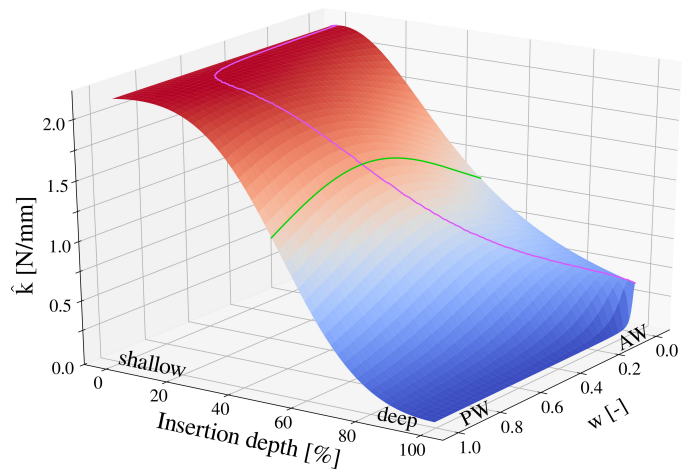


Figure 6: The maximum passive stiffness  $\hat{k}$  as function of instrument insertion depth and wrist weighting factor  $w$ . The magenta line indicates the optimal wrist weighting factor  $\hat{w}$  at each insertion depth. The green line gives the profile for  $\hat{k}$  as a function of  $w$  for an instrument that is halfway inserted. The deviation from the trend towards PW at shallow depths results from the specific 6-DoF robot kinematics  $\mathbf{J}_r \neq \mathbf{I}$ .

can be maximized for every configuration. However, care has to be taken not to inject energy in the system due to variations in the stiffness that the individual actuators have to render. Adverse effects from such energy injection may be avoided by introducing a certain safety factor on  $\hat{k}$  or by relying on the additional physical dissipation that is provided by the human operator and the body wall contact at the incision point (both considered to be passive). Alternatively, passivity observers and passivity controllers [34], or tank-based approaches [35] may be pursued to monitor and dissipate the excess of energy.

### C. Virtual Wall Stability

The increased stability for rendering a virtual wall at the distal tip with the proposed hybrid method has been experimentally validated. In these experiments, the wall was rendered according to the AW, PW and hybrid strategy. In the latter, the optimal wrist weighting factor was computed in real-time. An operator was asked to interact with the wall by manipulating the instrument at its handle. Given a specific configuration of the Virtuose6D and a virtual wall of a stiffness  $k$ , it was observed that the optimal wrist weighting factor of the hybrid method lead to stable interaction at a higher (or equal)  $k$ , when compared to AW or PW control. As discussed before, the stability increase is most prominent for instruments that are halfway inserted. Therefore, Fig. 7 presents results for an insertion depth of 60% and a wall stiffness of  $k = 1 \text{ N/mm}$ . The optimal wrist weighting factor  $\hat{w}$  was selected according to Fig. 7.a. Fig. 7.b demonstrates that, upon wall contact, limit cycles arise when  $w = 0$ , whereas large and unstable jerky motions occur when  $w = 1$ . Both effects are avoided with the hybrid method, where  $w = \hat{w}$ .

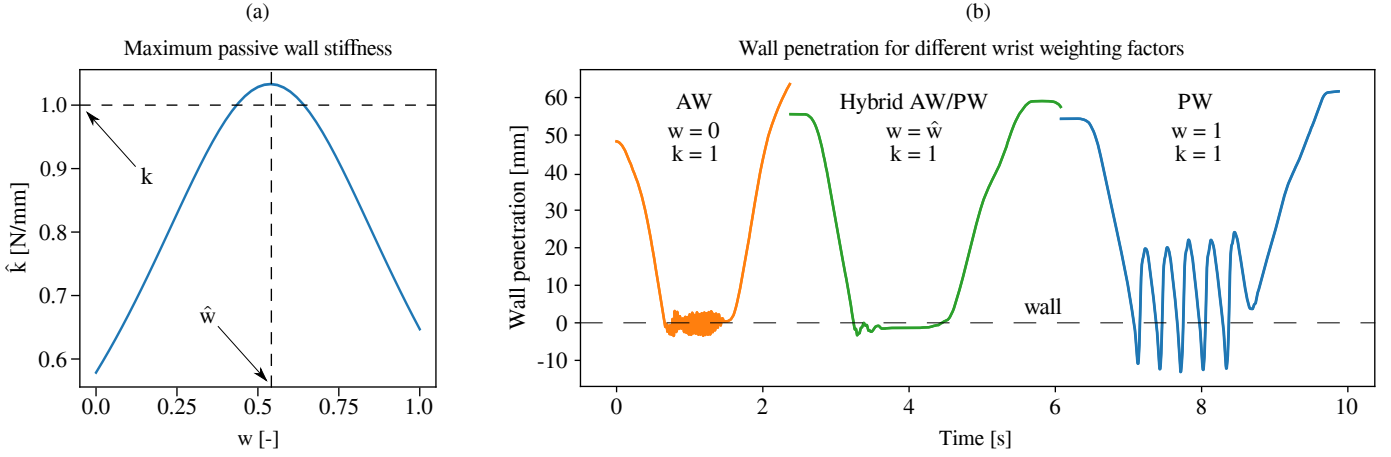


Figure 7: (a) Selection of the optimal wrist weighting factor  $\hat{w}$  that maximizes the passive wall stiffness  $\hat{k}$ . (b) Penetration depth through a virtual wall of stiffness  $k = 1$  N/mm, for different wrist weighting factors  $w$ , corresponding to the different discussed control strategies. This shows the impact of the choice of  $w$  on the wall stability.

## VI. CONCLUSION

This letter describes a method for rendering improved virtual fixtures at the distal tip of a surgical instrument using backdrivable, wristed comanipulation robots. The wrist of these robots may be either active or passive. Although passive wrist approaches are attractive due to their reduced mechanical complexity, they show shortcomings when it comes to rendering distal virtual fixtures. Especially when the instrument is inserted more than halfway, the fulcrum effect becomes problematic. It is shown that in such case the incapability to produce wrist moments negatively affects the stability of the virtual fixture or, equivalently, the maximum passive virtual fixture stiffness. Active wrist approaches are found to be less susceptible to this problem.

A hybrid active/passive wrist control strategy was proposed to compensate for the shortcomings of the separate control strategies. The developed optimization algorithm provides an appropriate weighting factor that distributes the actuator effort over a number of redundant actuators. The distribution is optimized such that the Z-width of the individual actuators is optimally leveraged. In an analytical example, it is shown that the result of the optimization algorithm is in agreement with the underlying intuition. Finally, it is experimentally confirmed that the hybrid method increases virtual fixture stability.

Suggestions for future work include investigating the impact of continuous stiffness adaptation on user perception and performance, as well as the possibility to modulate the fulcrum scaling factor  $s_f$  in order to facilitate stable VF rendering.

## APPENDIX

### SOLVING THE OPTIMIZATION PROBLEM

In this appendix, an analytical solution to the optimization problem (39) is derived. This implies finding the minimum of the function:

$$f(w_x, w_y) = \mathbf{v}^T \mathbf{K}_a^{-1} \mathbf{v}. \quad (45)$$

As a first step, let  $\mathbf{w}$  and  $\mathbf{W}$  be:

$$\mathbf{w} = [w_x \quad w_y \quad 1]^T, \quad (46)$$

$$\mathbf{W} = \mathbf{I} \odot \mathbf{1}\mathbf{w}^T, \quad (47)$$

with  $\odot$  the operator of the Schur product,  $\mathbf{I}$  the identity matrix and  $\mathbf{1} = [1 \quad 1 \quad 1]^T$ . Next, the dependence of  $\mathbf{J}_p$  on  $\mathbf{W}$  is made explicit. Starting from (9), this yields:

$$\mathbf{J}_p = \begin{bmatrix} w_x & 0 & 0 & 0 & w_x l_o - l_o & 0 \\ 0 & w_y & 0 & -w_y l_o + l_o & 0 & 0 \\ 0 & 0 & 1 & 0 & 0 & 0 \end{bmatrix}, \quad (48)$$

$$= \begin{bmatrix} w_x & 0 & 0 \\ 0 & w_y & 0 \\ 0 & 0 & 1 \end{bmatrix} \begin{bmatrix} 1 & 0 & 0 & 0 & l_o & 0 \\ 0 & 1 & 0 & -l_o & 0 & 0 \\ 0 & 0 & 1 & 0 & 0 & 0 \end{bmatrix} + \begin{bmatrix} 0 & 0 & 0 & 0 & -l_o & 0 \\ 0 & 0 & 0 & l_o & 0 & 0 \\ 0 & 0 & 0 & 0 & 0 & 0 \end{bmatrix}, \quad (49)$$

$$= \mathbf{W}^T \mathbf{J}_{p,w} + \mathbf{J}_{p,c}. \quad (50)$$

Inserting (50) into (34) gives:

$$\mathbf{v} = \mathbf{J}_r^T (\mathbf{J}_{p,w}^T \mathbf{W} + \mathbf{J}_{p,c}^T) \mathbf{J}_f^T \mathbf{R}_d \mathbf{e}_z, \quad (51)$$

$$= \mathbf{J}_r^T \mathbf{J}_{p,w}^T \mathbf{W} \mathbf{J}_f^T \mathbf{R}_d \mathbf{e}_z + \mathbf{J}_r^T \mathbf{J}_{p,c}^T \mathbf{J}_f^T \mathbf{R}_d \mathbf{e}_z, \quad (52)$$

$$= \mathbf{J}_r^T \mathbf{J}_{p,w}^T \mathbf{I} \odot \mathbf{1}\mathbf{w}^T \mathbf{J}_f^T \mathbf{R}_d \mathbf{e}_z + \mathbf{J}_r^T \mathbf{J}_{p,c}^T \mathbf{J}_f^T \mathbf{R}_d \mathbf{e}_z \mathbf{e}_z^T \mathbf{w}, \quad (53)$$

$$= \mathbf{J}_r^T \mathbf{J}_{p,w}^T \mathbf{I} \odot (\mathbf{J}_f^T \mathbf{R}_d \mathbf{e}_z)^T \mathbf{w} + \mathbf{J}_r^T \mathbf{J}_{p,c}^T \mathbf{J}_f^T \mathbf{R}_d \mathbf{e}_z \mathbf{e}_z^T \mathbf{w}, \quad (54)$$

$$= (\mathbf{J}_r^T \mathbf{J}_{p,w}^T \mathbf{I} \odot \mathbf{1} (\mathbf{J}_f^T \mathbf{R}_d \mathbf{e}_z)^T + \mathbf{J}_r^T \mathbf{J}_{p,c}^T \mathbf{J}_f^T \mathbf{R}_d \mathbf{e}_z \mathbf{e}_z^T) \mathbf{w}, \quad (55)$$

$$= \mathbf{C}\mathbf{w}. \quad (56)$$

This result can be substituted in (45):

$$f(w_x, w_y) = (\mathbf{C}\mathbf{w})^T \mathbf{K}_a^{-1} \mathbf{C}\mathbf{w}, \quad (57)$$

$$= \mathbf{w}^T \mathbf{C}^T \mathbf{K}_a^{-1} \mathbf{C}\mathbf{w}, \quad (58)$$

$$= \mathbf{w}^T \mathbf{Q}\mathbf{w}. \quad (59)$$

It can be seen that (59) describes a bivariate quadratic function of the form:

$$f(w_x, w_y) = Aw_x^2 + Bw_xw_y + Cw_y^2 + Dw_x + Ew_y + F, \quad (60)$$

where

$$\mathbf{Q} = \begin{bmatrix} A & B/2 & D/2 \\ B/2 & C & E/2 \\ D/2 & E/2 & F \end{bmatrix}. \quad (61)$$

If  $B^2 - 4AC < 0$ , the function  $f(w_x, w_y)$  forms an elliptic paraboloid which has a minimum if  $A > 0$ . In practice, both conditions are satisfied and the minimum of  $f$  is located at:

$$\hat{w}_x = \frac{BE - 2CD}{4AC - B^2}, \quad (62)$$

$$\hat{w}_y = \frac{DB - 2AE}{4AC - B^2}. \quad (63)$$

These expressions for the wrist weighting factors express the solution to the optimization problem (39). The maximum passive wall stiffness  $\hat{k}$  becomes:

$$\hat{k} = f(\hat{w}_x, \hat{w}_y)^{-1}. \quad (64)$$

#### REFERENCES

- [1] L. H. Clark, P. T. Soliman, D. Odetto, M. S. Munsell, K. M. Schmeler, N. Fleming, S. N. Westin, A. M. Nick, and P. T. Ramirez, "Incidence of trocar site herniation following robotic gynaecologic surgery," *Gynecologic Oncology*, vol. 131, no. 2, pp. 400–403, 2013.
- [2] M. Jakopcic, S. J. Harris, F. R. y Baena, P. Gomes, and B. L. Davies, "The acrobot system for total knee replacement," *Industrial Robot: An International Journal*, vol. 30, no. 1, pp. 61–66, 2003.
- [3] A. Uneri, M. Balicki, J. Handa, P. Gehlbach, R. Taylor, and I. Iordachita, "New steady-hand eye robot with micro-force sensing for vitreoretinal surgery," in *Biomedical Robotics and Biomechanics (BioRob), 2010 3rd IEEE RAS and EMBS International Conference on*, sept. 2010, pp. 814–819.
- [4] A. Gijbels, E. B. Vander Poorten, P. Stalmans, and D. Reynaerts, "Development and experimental validation of force sensing needle for robotically assisted retinal vein cannulations," in *IEEE International Conference on Robotics and Automation*, 2015, pp. 2270–2276.
- [5] S. Voros, G. P. Haber, J. F. Menuudet, J. A. Long, and P. Cinquin, "Viky robotic scope holder: Initial clinical experience and preliminary results using instrument tracking," *IEEE/ASME Trans. Mechatron.*, vol. 15, no. 6, pp. 879–886, 2010.
- [6] N. Zemitl, G. Morel, T. Ortmaier, and N. Bonnet, "Mechatronic design of a new robot for force control in minimally invasive surgery," *IEEE/ASME Trans. Mechatron.*, vol. 12, no. 2, pp. 143–153, 2007.
- [7] B. Rosa, E. Vander Poorten, C. Gruijthuijsen, J. Vander Sloten, and D. Reyaerts, "Localization of pivot point into the patient body for automatic RCM alignment in robotic MIS surgery," in *Computer Assisted Radiology and Surgery 28th International Congress*, 2014.
- [8] U. Hagn, T. Ortmaier, R. Konietschke, B. Kubler, U. Seibold, A. Toberge, M. Nickl, S. Jorg, and G. Hirzinger, "Telem manipulator for remote minimally invasive surgery," *IEEE Robot. Automat. Mag.*, vol. 15, no. 4, 2008.
- [9] B. Herman, B. Dehez, K. T. Duy, B. Raucent, E. Dombre, and S. Krut, "Design and preliminary in vivo validation of a robotic laparoscope holder for minimally invasive surgery," *The International Journal of Medical Robotics and Computer Assisted Surgery*, vol. 5, no. 3, 2009.
- [10] R. Polet and J. Donnez, "Gynecologic laparoscopic surgery with a palm-controlled laparoscope holder," *The Journal of the American Association of Gynecologic Laparoscopists*, vol. 11, pp. 73–78, 2004.
- [11] J. M. Sackier and Y. Wang, "Robotically assisted laparoscopic surgery," *Surgical Endoscopy*, vol. 8, no. 1, pp. 63–66, 1994.
- [12] C. Poquet, P. Mozer, G. Morel, and M.-A. Vitrani, "A novel manipulation device for assisting needle placement in ultrasound guided prostate biopsies," in *2013 IEEE/RSJ International Conference on Intelligent Robots and Systems*, 2013, pp. 4084–4091.
- [13] L. Dong and G. Morel, "Robust trocar detection and localization during robot-assisted endoscopic surgery," in *2016 IEEE International Conference on Robotics and Automation*, 2016, pp. 4109–4114.
- [14] C. Gruijthuijsen, L. Dong, G. Morel, and E. V. Poorten, "Leveraging the fulcrum point in robotic minimally invasive surgery," *IEEE Robotics and Automation Letters*, vol. 3, no. 3, pp. 2071–2078, 2018.
- [15] L. Rosenberg, "Virtual fixtures: Perceptual tools for telerobotic manipulation," in *Proceedings of IEEE Virtual Reality Annual International Symposium*, 1993, pp. 76–82.
- [16] A. M. Okamura, "Haptic feedback in robot-assisted minimally invasive surgery," *Current Opinion in Urology*, vol. 19, pp. 102–107, 2009.
- [17] J. J. Abbott, P. Marayong, and A. M. Okamura, "Haptic virtual fixtures for robot-assisted manipulation," in *Robotics Research*, S. Thrun, R. Brooks, and H. Durrant-Whyte, Eds., 2007, pp. 49–64.
- [18] S. A. Bowyer, B. L. Davies, and F. Rodriguez y Baena, "Active constraints/virtual fixtures: A survey," *IEEE Transactions on Robotics*, vol. 30, no. 1, pp. 138–157, 2014.
- [19] M.-A. Vitrani, C. Poquet, and G. Morel, "Applying virtual fixtures to the distal end of a minimally invasive surgery instrument," *IEEE Transactions on Robotics*, vol. 33, no. 1, pp. 114–123, 2017.
- [20] C. Gruijthuijsen, R. Colchester, A. Devreker, A. Javaux, D. Stoyanov, D. Reynaerts, J. Deprest, S. Ourselin, A. Desjardins, T. Vercauteren, and E. Vander Poorten, "Haptic guidance based on all-optical ultrasound distance sensing for safer minimally invasive fetal surgery," *Journal of Medical Robotics Research*, vol. 3, no. 3, pp. 1–19, 2018.
- [21] L. Dong, "Assistance to laparoscopic surgery through comanipulation," Ph.D. dissertation, Université Pierre et Marie Curie, Paris, 2017.
- [22] T. Xia, C. Baird, G. Jallo, K. Hayes, N. Nakajima, N. Hata, and P. Kazanzides, "An integrated system for planning, navigation and robotic assistance for skull base surgery," *Int J Med Robot*, vol. 4, no. 4, pp. 321–30, 2008.
- [23] F. Rydén and H. J. Chizeck, "Forbidden-region virtual fixtures from streaming point clouds: Remotely touching and protecting a beating heart," in *2012 IEEE/RSJ International Conference on Intelligent Robots and Systems*, 2012, pp. 3308–3313.
- [24] J. Jang, H. W. Kim, and Y. S. Kim, "Construction and verification of a safety region for brain tumor removal with a telesurgical robot system," *Minimally Invasive Therapy & Allied Technologies*, vol. 23, no. 6, pp. 333–340, 2014.
- [25] N. Colonnese and A. Okamura, "Stability and quantization-error analysis of haptic rendering of virtual stiffness and damping," *The International Journal of Robotics Research*, vol. 35, no. 9, pp. 1103–1120, 2016.
- [26] D. W. Weir and J. E. Colgate, "Stability of haptic displays," in *Haptic Rendering: Foundations, Algorithms, and Applications*, M. C. Lin and M. Otaduy, Eds. AK Peters, 2008, pp. 123–156.
- [27] S. A. Bowyer and F. Rodriguez y Baena, "Dissipative control for physical human-robot interaction," *IEEE Transactions on Robotics*, vol. 31, no. 6, pp. 1281–1293, 2015.
- [28] A. G. Gallagher, N. McClure, J. McGuigan, K. Ritchie, and N. P. Sheehy, "An ergonomic analysis of the fulcrum effect in the acquisition of endoscopic skills," *Endoscopy*, vol. 30, no. 07, pp. 617–620, 1998.
- [29] S. Sülzenbrück and H. Heuer, "Learning the visuomotor transformation of virtual and real sliding levers: simple approximations of complex transformations," *Experimental Brain Research*, vol. 195, no. 1, pp. 153–165, 2009.
- [30] I. Nisky, F. Huang, A. Milstein, C. Pugh, F. Mussa-Ivaldi, and A. Karniel, "Perception of stiffness in laparoscopy: the fulcrum effect," *Studies in health technology and informatics*, vol. 173, pp. 313–319, 2012.
- [31] J. E. Colgate and G. Schenkel, "Passivity of a class of sampled-data systems: application to haptic interfaces," in *Proceedings of 1994 American Control Conference - ACC '94*, vol. 3, 1994, pp. 3236–3240.
- [32] B. E. Miller, J. E. Colgate, and R. A. Freeman, "On the role of dissipation in haptic systems," *IEEE Transactions on Robotics*, vol. 20, no. 4, pp. 768–771, 2004.
- [33] S. Boyd and L. Vandenberghe, *Convex Optimization*. Cambridge University Press, 2004.
- [34] B. Hannaford and J.-H. Ryu, "Time-domain passivity control of haptic interfaces," *IEEE Transactions on Robotics and Automation*, vol. 18, no. 1, pp. 1–10, 2002.
- [35] M. Selvaggio, G. A. Fontanelli, F. Ficuciello, L. Villani, and B. Siciliano, "Passive virtual fixtures adaptation in minimally invasive robotic surgery," *IEEE Robotics and Automation Letters*, vol. 3, no. 4, pp. 3129–3136, 2018.